

Numerical Predictions of Pressure Fluctuations in a Model Pump Turbine with Small Guide Vane Opening based on Partial Averaged Navier Stokes Approach

J. T. Liu^{1†}, Y. L. Wu² and Y. Li²

¹ *Beijing Institute of Control Engineering, Beijing, 100190, China*

² *Department of Thermal Engineering, Tsinghua University, Beijing 100084, China*

†*Corresponding Author Email: liujintao86@hotmail.com*

(Received December 20, 2015; accepted March 10, 2016)

ABSTRACT

Comparing with conventional hydraulic turbine (e.g. Francis turbine), pump turbine shows significant unstable characteristics because its design is a compromise between a pump and a turbine. In present paper, unsteady flow and pressure fluctuations within a model pump turbine are numerically studied through Partial Averaged Navier Stokes (PANS) approach. The PANS approach is fulfilled through modification of RNG k- ϵ turbulence model in a commercial CFD code. Pump turbine operating at different conditions with guide vanes opening angle 6° is simulated. Results revealed that the predictions of performance and relative peak-to-peak amplitude by PANS approach agree well with the experimental data. Velocity, vortex and turbulent kinetic energy at the inlet of runner are very large near the pressure surface and the blade leading edge, leading to high pressure fluctuations within the vaneless area of pump turbine. The maximum amplitude of pressure fluctuation occurs when the pump turbines run at runaway point. The primary dominant frequency of pressure fluctuation is the runner blade passing frequency in the vaneless space. The above high pressure fluctuations should be avoided during the design of pump turbines especially those operating at high-head condition.

Keywords: Pump turbine; Pressure fluctuation; Partial-Averaged Navier-Stokes; Unsteady flow.

NOMENCLATURE

D_I	runner inlet diameter in pump mode	x	coordinates
f_k	unresolved-to-total ratios of kinetic energy	Z_S	number of stay vanes
f_z	unresolved-to-total ratios of dissipations	Z_G	number of guide vanes
H_d	rated head	Z	number of runner blades
k	turbulent kinetic energy of RANS approach	ν	kinematic viscosity
k_u	turbulent kinetic energy of PANS approach	ϵ	turbulent dissipation of RANS approach
n	rotational speed of the runner	ϵ_u	turbulent dissipation of PANS approach
n_{11}	unit speed of the model pump turbine	ρ	density
p	pressure	μ	dynamic viscosity
P_k	production terms of turbulence kinetic energy	γ	relative opening of guide vanes of the pump turbine
Q_{11}	unit discharge of the model pump turbine	LES	Large Eddy Simulation
Q_d	rated discharge	$PANS$	Partially-Averaged Navier-Stokes
t	time	$URANS$	Unsteady Reynolds Averaged Navier-Stokes
T	turbulence time scale	FFT	Fast Fourier Transform
u_i	unresolved part of instantaneous velocity		
U	partially averaged velocity of instantaneous velocity		
\bar{U}	mean component of velocity		
v	turbulence velocity scale		
V	instantaneous velocity		

1. INTRODUCTION

Pumped-storage power plant is one of essential components for the development of renewable energy and the enhancement of electricity supply security. Among all the elements of the pumped-storage power plant, pump turbine is the most important one. Since design of the pump turbine is a compromise between a pump and a turbine, the performance of pump turbine always shows significant and unstable characteristics comparing with conventional hydroturbines (e.g. Francis turbine) with the same specific speed as shown in Fig. 1. If a pump turbine is operated within the “S” region (e.g. conditions during transient process of start-up, runaway and load rejection), oscillations under this operating conditions may cause the shift of pump turbine from turbine mode to the turbine braking mode, or even force the unit further into reverse pump mode, affecting its operational stability (Yamaguchi *et al.* 1984).

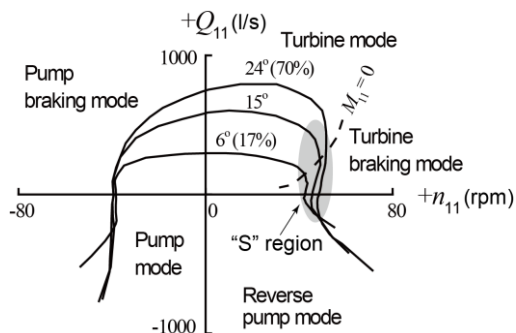


Fig. 1. Characteristics curves during operations of pump turbines.

One of the main reasons for the instability of turbine mode of pump turbine is that the optimum speed of turbine mode is not the same as one of pump mode. Since the speed of pump turbine is mainly governed by the pump mode performance, pump turbine will be operated at off-design conditions in its whole operational domain during the turbine mode. Therefore, a strong instability within pump turbine will be induced during operating at off-design conditions. Moreover, some unwished phenomena (e.g. structural vibrations, noises and cavitation) also occur at those off-design conditions. Staubli *et al.* (2008) predicted the characteristic of pump turbine near runaway and the flow phenomena leading to the instability at small flow rates. Hasmatuchi *et al.* (2009, 2011) experimentally and numerically investigated the hydrodynamics of a model pump turbine operated at off-design conditions (i.e. 5° and 10° guide vane openings). Yan *et al.* (2010, 2012) numerically studied the characteristic curve and the pressure fluctuation of a model pump-turbine with 10° guide vane opening.

In pump turbines, rotor-stator interaction is usually considered as the source of unsteady phenomena and dynamic fluctuations, especially at operation condition with high head (Jung *et al.* 2012, Wu *et al.* 2013). For example, the interaction between

impeller blades and guide vanes is one of the main causes of vibrations in pump turbines. Nicolet *et al.* (2006) modeled the one-dimensional rotor-stator interaction in pump-turbine. Zobeiri *et al.* (2006) numerically investigated the rotor-stator interactions of a model pump turbine in turbine mode for the maximum discharge operating conditions. The rotor-stator interaction can be considered as an interaction between potential and viscous flow and wakes. Those phenomena are of interest to improve the design turbine toward better efficiency at off-peak conditions (Wu *et al.* 2013).

For predictions of pressure fluctuations in hydraulic machinery, a three-dimensional flow simulation based on the Unsteady Reynolds Averaged Navier-Stokes (URANS) equations have been well discussed in the literature (Qian *et al.* 2010, Wu *et al.* 2011). Specifically for URANS approach in pump turbines, the unstable characteristics and pressure fluctuations in a pump turbine have been analyzed through using URANS (Huang *et al.* 2013, Wang *et al.* 2011). Yin *et al.* (2011, 2012) further studied the compressibility of water on the pressure fluctuations of pump turbine based on URANS approach. Liu *et al.* (2012, 2013) studied three-dimensional, unsteady and incompressible flows in a pump turbine during a transient process of load rejection using URANS approach with the nonlinear turbulence model to incorporate the near-wall turbulence anisotropy to improve the simulation accuracy.

Unfortunately, the aforementioned URANS approach couldn't capture the flow with all kinds of scales. Large Eddy Simulation (LES) could improve predictions but is not computationally economical due to the considerable high cost for engineering problems (e.g. simulations of whole passage of pump turbine). As an alternative, various hybrid RANS/LES approaches have been proposed. For example, a Partially-Averaged Navier-Stokes (PANS) approach, which changes seamlessly from RANS to the direct numerical solution of the Navier-Stokes equations, was proposed by Girimaji *et al.* (2003, 2006). Two variants of the PANS model are derived based on the $k-\epsilon$ formulation (Mirzaei *et al.* 2015, Shi *et al.* 2015) and the $k-\omega$ formulation (Srinivasan *et al.* 2014) respectively. Predictions of PANS have been found to be better than those of LES in the flow regions suffering from poor near-wall resolution during simulations (Lakshminpathy *et al.* 2004). Recently, Ji *et al.* (2013) studied the unsteady cavitating turbulence flow around a highly skewed model marine propeller based on the PANS approach.

In present paper, PANS approach based on the RNG $k-\epsilon$ formulation will be employed to simulate the unsteady flow through a model pump turbine operating at conditions with small guide vane opening. Experimental data of the model turbine are employed to validate the predictions (e.g. performance and relative peak-to-peak amplitude) by PANS approach. Unsteady phenomena (e.g. pressure fluctuations) are also studied to improve the design of pump turbine.

2. GOVERNING EQUATIONS

For incompressible flow, the continuity equation and Reynolds averaged Navier-Stokes equations are (Germano *et al.* 1992),

$$\frac{\partial U_i}{\partial t} + U_j \frac{\partial U_i}{\partial x_j} + \frac{\partial \tau(V_i, V_j)}{\partial x_j} = -\frac{\partial \langle p \rangle}{\partial x_i} + \nu \frac{\partial^2 U_i}{\partial x_j \partial x_j} \quad (1)$$

$$-\frac{\partial^2 \langle p \rangle}{\partial x_i \partial x_i} = -\frac{\partial U_i}{\partial x_j} \cdot \frac{\partial U_j}{\partial x_i} + \frac{\partial \tau(V_i, V_j)}{\partial x_i \partial x_j} \quad (2)$$

Here, \mathbf{V} is the instantaneous velocity (subscript i and j indicating components in different directions); \mathbf{U} is the partially averaged velocity; t is the time; p is the pressure; $\langle \rangle$ denotes a constant-preserving arbitrary (implicit or explicit) filter commuting with spatial and temporal differentiation; \mathbf{x} denotes the coordinates; ν is the kinematic viscosity. Here, V_i is partitioned into two parts: partially averaged velocity (U) unresolved part (u_i)

$$V_i = U_i + u_i \quad (3)$$

$$U_i = \langle V_i \rangle. \quad (4)$$

In Eqs. (1) and (2), the additional non-linear term $\tau(V_i, V_j)$ (i.e. the generalized central second moment) is defined as,

$$\tau(V_i, V_j) = \langle V_i V_j \rangle - \langle V_i \rangle \langle V_j \rangle. \quad (5)$$

In RNG k - ε turbulence mode, the equations for turbulent kinetic energy (k) and turbulent dissipation (ε) can be given as follows (Yakhot *et al.* 1992),

$$\frac{\partial (\rho k)}{\partial t} + \frac{\partial (\rho \overline{U_j k})}{\partial x_j} = \frac{\partial}{\partial x_j} \left[\alpha_k (\mu + \mu_t) \frac{\partial k}{\partial x_j} \right] + P_k - \rho \varepsilon \quad (6)$$

$$\begin{aligned} \frac{\partial (\rho \varepsilon)}{\partial t} + \frac{\partial (\rho \overline{U_j \varepsilon})}{\partial x_j} &= \frac{\partial}{\partial x_j} \left[\alpha_\varepsilon (\mu + \mu_t) \frac{\partial \varepsilon}{\partial x_j} \right] - \\ &+ C_{\varepsilon 1}^* P_k \frac{\varepsilon}{k} - C_{\varepsilon 2}^* \rho \frac{\varepsilon^2}{k} \end{aligned} \quad (7)$$

where,

$$\mu_t = \rho C_\mu \frac{k^2}{\varepsilon} \quad C_{\varepsilon 1}^* = C_{\varepsilon 1} - \frac{\eta(1-\eta/\eta_0)}{1+\beta\eta^3}$$

$$S_{ij} = \frac{1}{2} \left(\frac{\partial \overline{U_i}}{\partial x_j} + \frac{\partial \overline{U_j}}{\partial x_i} \right) \quad \eta = (2S_{ij} \cdot S_{ij})^{1/2} \frac{k}{\varepsilon}$$

with $C_\mu = 0.0845$, $\alpha_k = \alpha_\varepsilon = 1.39$, $C_{\varepsilon 1} = 1.42$, $C_{\varepsilon 2} = 1.68$, $\eta_0 = 4.377$, $\beta = 0.012$. In Eqs. (6) and (7), ρ is the density; $\overline{\mathbf{U}}$ is the mean component of velocity; μ is the dynamic viscosity; P_k denotes the production terms of turbulence kinetic energy.

As shown in Girimaji *et al.* (2006), the extent of PANS averaging relative to RANS can be quantified using the unresolved-to-total ratios of kinetic energy (f_k) and dissipations (f_ε),

$$f_k = \frac{k_u}{k} \quad f_\varepsilon = \frac{\varepsilon_u}{\varepsilon}$$

The relationship between P_k in RNG k - ε turbulence mode and P_{ku} in PANS model can be obtained through equating the source terms such as,

$$P_k = \frac{1}{f_k} (P_{ku} - \varepsilon_u) + \frac{\varepsilon_u}{f_\varepsilon} \quad (9)$$

Then we can obtain PANS model by the modification of RNG k - ε turbulence model with the following equations,

$$\begin{aligned} \frac{\partial (\rho k_u)}{\partial t} + \frac{\partial (\rho \overline{U_j k_u})}{\partial x_j} &= \\ \frac{\partial}{\partial x_j} \left[\alpha_k \left(\mu + \frac{\mu_u}{\sigma_u} \right) \frac{\partial k_u}{\partial x_j} \right] &+ P_{ku} - \rho \varepsilon_u \end{aligned} \quad (10)$$

$$\begin{aligned} \frac{\partial (\rho \varepsilon_u)}{\partial t} + \frac{\partial (\rho \overline{U_j \varepsilon_u})}{\partial x_j} &= \frac{\partial}{\partial x_j} \left[\alpha_\varepsilon \left(\mu + \frac{\mu_u}{\sigma_u} \right) \frac{\partial \varepsilon_u}{\partial x_j} \right] \\ &+ C_{\varepsilon 1}^* P_{ku} \frac{\varepsilon_u}{k_u} - C_{\varepsilon 2}^* \rho \frac{\varepsilon_u^2}{k_u} \end{aligned} \quad (11)$$

$$\text{with} \quad \mu_u = \rho C_\mu \frac{k_u^2}{\varepsilon_u} \quad (12)$$

$$\sigma_{ku} = \frac{f_k^2}{f_\varepsilon}, \quad \sigma_{\varepsilon u} = \frac{f_\varepsilon^2}{f_k} \quad (13)$$

$$C_{\varepsilon 2}^* = C_{\varepsilon 1}^* + \frac{f_k}{f_\varepsilon} (C_{\varepsilon 2} - C_{\varepsilon 1}^*) \quad (14)$$

where,

$$C_\mu = 0.0845, \quad \alpha_k = \alpha_\varepsilon = 1.39, \quad C_{\varepsilon 1} = 1.42, \quad \eta_0 = 4.377, \quad \beta = 0.012.$$

Considering the nonlinear turbulence flow in the pump turbine, the shear stress was solved by nonlinear turbulence model which was proposed by Ehrhard *et al.* (1999),

$$P_k = -\overline{\rho U_i' U_j'} \frac{\partial \overline{U_j}}{\partial x_j} \quad (15)$$

$$\begin{aligned} \overline{U_i' U_j'} &= \frac{2}{3} k \delta_{ij} - 2C_{\mu P} \nu^2 T S_{ij} \\ &+ C_1 C_{\mu P} \nu^2 T^2 \left(S_{ik} S_{kj} - \frac{1}{3} S_{kl} S_{kl} \delta_{ij} \right) \\ &+ C_2 C_{\mu P} \nu^2 T^2 \left(\Omega_{ik} S_{kj} - \Omega_{jk} S_{ki} \right) \\ &+ C_3 C_{\mu P} \nu^2 T^2 \left(\Omega_{ik} \Omega_{jk} - \frac{1}{3} \Omega_{ik} \Omega_{ik} \delta_{ij} \right) \\ &+ C_4 C_{\mu P} \nu^2 T^3 \left(S_{ki} \Omega_{lj} - S_{kj} \Omega_{li} \right) S_{kl} \\ &+ C_5 C_{\mu P} \nu^2 T^3 S_{ij} S_{kl} S_{kl} + C_6 C_{\mu P} \nu^2 T^3 S_{ij} \Omega_{kl} \Omega_{kl} \end{aligned} \quad (16)$$

and

$$C_{\mu P} = \min\left(\frac{1}{0.9S^{1.4} + 0.4\Omega^{1.4} + 3.5}, 0.15\right);$$

$$\Omega_{ij} = \frac{1}{2}\left(\frac{\partial \bar{U}_i}{\partial x_j} + \frac{\partial \bar{U}_j}{\partial x_i}\right); S = \frac{k}{\varepsilon} \sqrt{2S_{ij}S_{ij}};$$

$$\Omega = \frac{k}{\varepsilon} \sqrt{2\Omega_{ij}\Omega_{ij}}$$

where $C_{\mu ke} = \beta \frac{k^2}{\varepsilon}$, $C_1 = -0.2$, $C_2 = 0.4$,
 $C_3 = 2.0 - \exp(-(S - \Omega)^2)$, $C_4 = -32.0C_{\mu P}^2$,
 $C_5 = -16.0C_{\mu P}^2$, $C_6 = 16.0C_{\mu P}^2$. In Eq. (16), T is the turbulence time scale and V is the turbulence velocity scale.

3. GEOMETRY OF PUMP TURBINE

In present paper, a model pump turbine with the parameters shown in Table 1 will be investigated. In Table 1. The structure of pump turbine is shown in Fig. 2a. In present paper, the relative opening (γ) of guide vanes of the pump turbine is 6° . Fig. 2b shows the meridian line of the runner obtained from the hydraulic design. The surface formed by the meridian line of the runner rotating on Z axial is termed as ‘‘S1’’ surface. The simulated results on the S1 surface will be shown in the following sections.

Table 1 Parameters of the model pump turbine simulated

Rated head H_d (m)	60.6
Rated floe rate Q_d (m ³ /s)	0.25
Rotational speed n (rpm)	1200
Runner outlet diameter D_1 (m)	0.24
Number of runner blade Z	9
Number of stay vanes Z_s	20
Number of guide vanes Z_G	20

The experimental data shown in present paper were acquired through the model tests. The pressure fluctuations at the inlet of case and the outlet of draft tube were obtained by pressure sensors during the tests. The head can be calculated based on the pressure difference between the inlet of case and the outlet of draft tube. The rotation speed of the runner and the flow rate of the pump turbine were measured by revolution speed transducer and flow measurement device respectively.

3.1 Boundary Conditions

In present paper, the following boundary conditions are employed to investigate the turbulent flow in the pump turbine, (1) At the inlet of the flow domain, definite values of all physical

variants are prescribed. (2) At the outlet, the gradients of all physical variants normal to the boundaries are given. (3) On solid walls of the domain, the non-slip flow condition is adopted and near the solid walls, the enhanced wall treatment is employed. (4) Zero pressure gradient normal to the surface is employed for all boundaries of the domain except a point corresponding to the reference pressure.

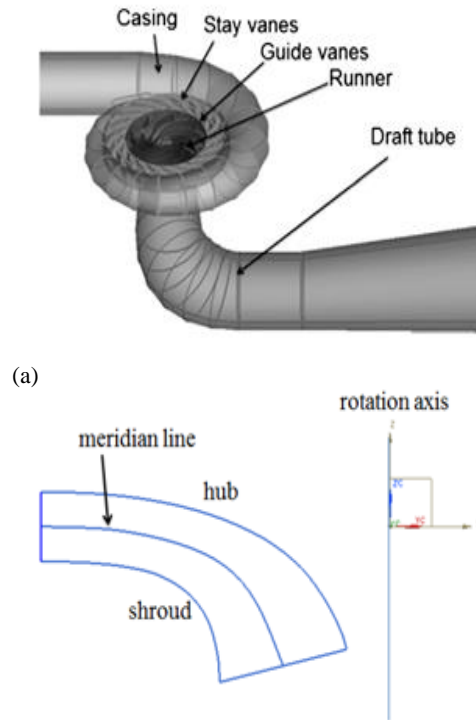


Fig. 2. Geometry profile of the simulated pump turbine.

To satisfy the continuity condition, correction of velocity magnitude to the outlet distribution is made based on the difference between the inflow and the outflow during the simulation (Wu *et al.* 2011).

3.2 Simulation of Unsteady Flow at Turbine Mode

In this section, turbulent flow through the model pump turbine at turbine model will be simulated. Fig. 2 shows the whole flow passage of pump turbine (including spiral case, stay vanes, guide vanes, runner and draft tube) to be simulated.

The SIMPLEC algorithm was used to enforce mass conservation. For the quad/hex grids and complex flows in turbine mode, a second-order center difference was employed for the pressure interpolation and a second-order upwind difference was employed for the terms of momentum equations and terms of two new sets of scalar equations to improve accuracy. The flow was assumed to be converged when the residual error is less than 0.0001.

In the PANS Solution, we assumed $f_k=0.2$ and $f_\varepsilon=1$ (Huang *et al.* 2013).The relaxation factor settings

were as follows: momentum and pressure term is 0.3; density term is 1; turbulent viscous term is 0.8; and a new two scalar relaxation factor is 1. For unsteady simulation, the Courant number was controlled to be below 10. Time step for the runner rotation were controlled to be 1° rotation of runner in each time step. The number of iterative simulations in each time step is set to be 100. Mesh independency has been investigated and mesh with about 9 million cells in total was chosen for the simulations.

4. RESULTS AND DISCUSSIONS

4.1 Books and Theses

Figure 3 shows the comparisons of performance curve of the model pump turbine at the turbine mode with 6° opening of the guide vanes between experimental data (“Solid line”) and our predictions (“Open circle”). In Fig. 3, points G1 and G6 correspond to the maximum flow rate point and zero flow rate point respectively. For simulations at each point, the rotational speed of runner was set as a constant and the flow rate was adjusted by setting the boundary condition (e.g. velocity) at the inlet of the pump turbine. With the head of pump turbine determined, the unit speed (n_{11}) and unit discharge (Q_{11}) of the model pump turbine could be calculated using the following formula,

$$n_{11} = \frac{nD_1}{\sqrt{H}} ; \quad Q_{11} = \frac{Q}{D_1^2 \sqrt{H}}$$

Based on Fig. 3, it is clear that the predictions agree well with the test data at G1 to G6 operation cases for the turbine mode.

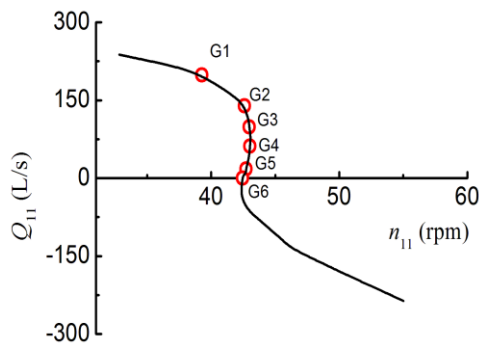


Fig. 3. Performance curve of the model pump turbine.

The prediction results of performance at G1 to G6 conditions on the guide vanes’ opening angle are listed in Table 2.

4.2 Pressure Fluctuation in the Vaneless Space

In this section, the amplitude and dominant frequency of pressure fluctuation at vaneless space between the runner and guide vane of the pump turbine will be investigated. In the literature, some of experimental and numerical research works have

been focused on the pressure fluctuations at vaneless space, especially for small flow rate case (Hasmatuchi *et al.* 2011, Yan *et al.* 2010), and even during the design stage (Jung *et al.* 2012). Because there exist strong interactions between the runner and the guide vanes of the pump turbine, the separation flow phenomenon and the rotating stall will happen at small flow rate operating conditions under the turbine mode.

Table 2 Different points for calculations at the guide vanes’ opening angle 6°

No.	n_{11} (rpm)	Q_{11} (L/s)
G1	39.27	198.38
G2	42.59	139.17
G3	42.97	98.63
G4	43.03	61.46
G5	42.72	17.55
G6	42.46	0

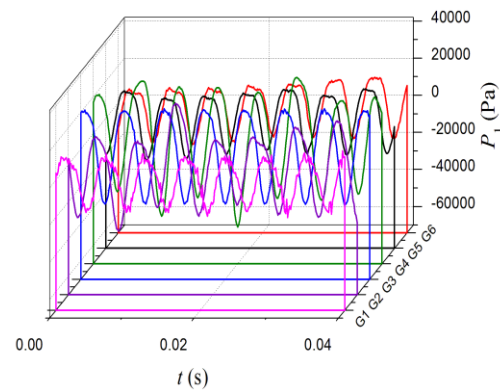
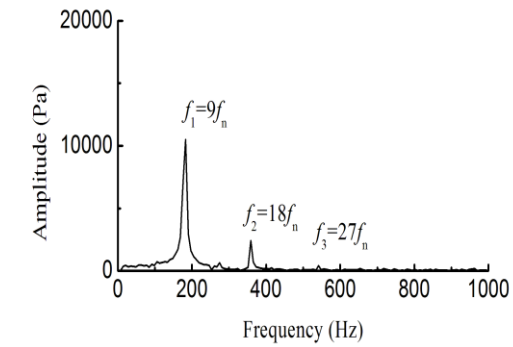


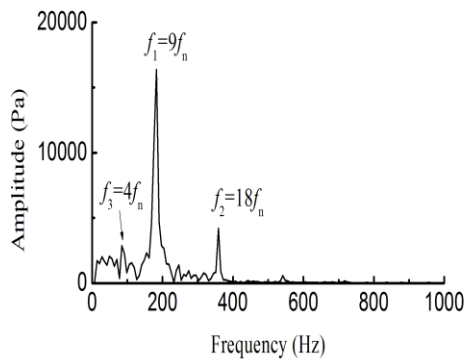
Fig. 4. Pressure fluctuations versus time at the operating conditions G1 to G6.

Figure 4 shows the pressure fluctuations in the vaneless space at time domain under the operating conditions G1 to G6. The amplitude of the pressure fluctuation in the pump turbine at these points is consistent. Table 2 shows the comparisons between the predicted amplitudes and the experimental data of model test. The amplitude is measured in the time domain from peak to peak values with 97% reliability. The agreement between predictions and experiments is considerably good. Furthermore, both test and calculation have the same trends when pump turbine is operated from case G1 to case G6. In Table 3, the amplitude of pressure fluctuations increases from case G1 to case G4. Therefore, when pump turbine starts from the best efficiency case G1, with the increase of the unit speed, a significant increase of the amplitude of pressure fluctuations is observed in vaneless space between runner and guide vanes. At the runaway (corresponding to zero load), the amplitude of case G4 is maximum. The amplitude gradually

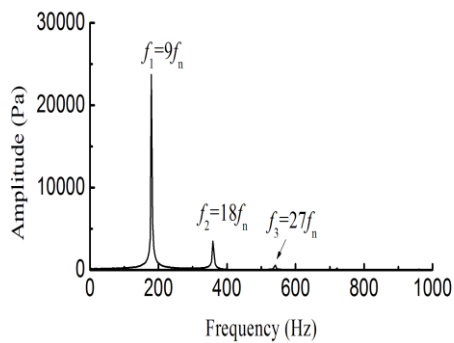
decreases from case G4 to case G5 (corresponding to turbine break case), then to case G6 (corresponding to zero flow rate). The above predicted trend of amplitude is nearly the same as experimental results by Hasmatuchi *et al.* (2009).



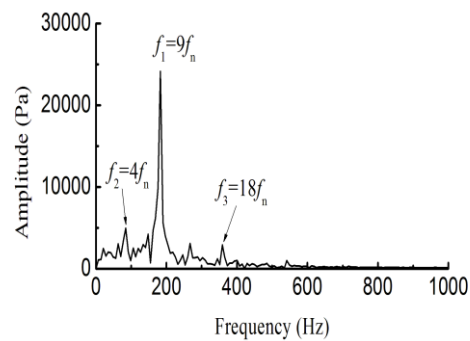
(a) G1



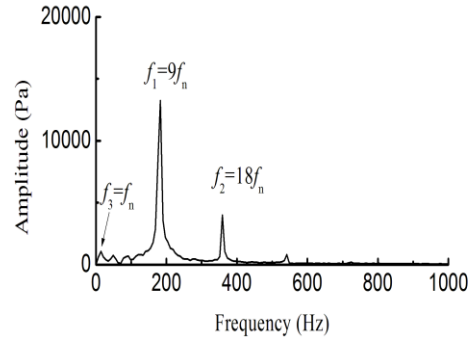
(b) G2



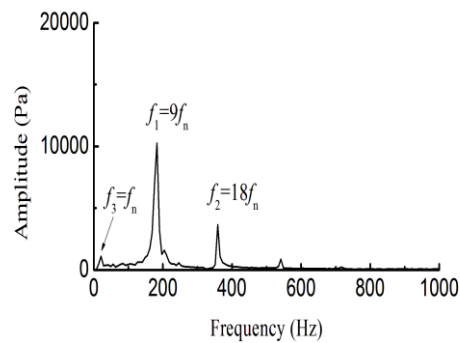
(c) G3



(d) G4



(e) G5



(f) G6

Fig. 5. Pressure fluctuation on the measured points G1 to G6 at frequency domain (corresponding to (a)-(f)) in the frequency domain. f_1 , f_2 and f_3 indicate the primary, secondary and third dominant frequency in the domain and their relationship with the frequency of the rotating runner (f_n).

Table 3 Comparison of predicted amplitudes of the model pump turbine with experimental data (A is amplitude).

	f_1	$\Delta H/H$ (%)		A at $9f_n$ (Pa)	A at $18f_n$ (Pa)
		Cal.	Exp.		
G1	9	5.6	5.1	10484.5	2405.2
G2	9	8.4	7.8	16367.8	4204.0
G3	9	7.9	8.3	23712.7	3468.1
G4	9	10.6	9.6	24126.6	2886.4
G5	9	7.2	7.9	13237.4	3984.3
G6	9	6.3	5.6	10272.2	3636.7

The pressure fluctuations data in time domain (e.g. Fig. 4) is transformed into frequency spectrum in frequency domain through Fast Fourier Transform (FFT) as shown in Fig. 5. The primary dominant frequency of pressure fluctuation is the runner blade passing frequency and the secondary dominant frequency is double of the runner blade passing frequency. Furthermore, the secondary dominant frequency is nearly equal to guide vane passing frequency.

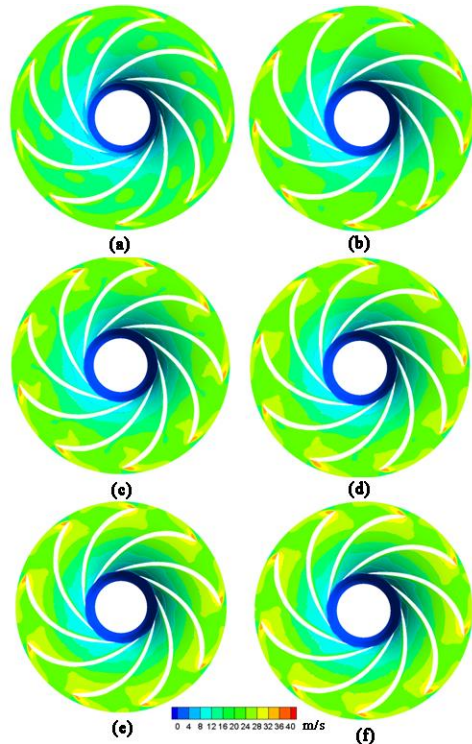


Fig. 6. Relative velocity distributions on the S1 stream surface of runner at different operating conditions G1-G6 (corresponding to (a)-(f) respectively).

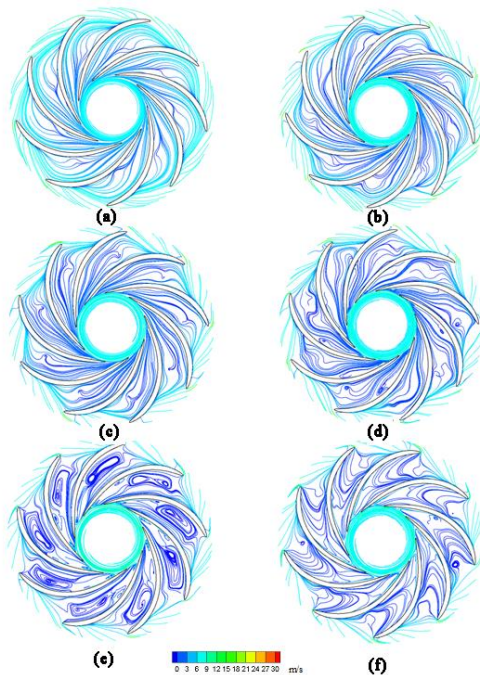


Fig. 7. Relative stream lines on the S1 stream surface of runner at different operating conditions G1-G6 (corresponding to (a)-(f) respectively).

Figures 6-8 show the relative velocity distributions, relative stream lines and vortex distributions on the

S1 stream surface of runner at different operation cases. Fig. 9 only shows the turbulent kinetic energy distribution at the case G1. As shown in Fig. 6, the relative velocity is obviously higher near the blade suction surface of the runner blade passages. At the zero flow rate case in Fig. 7f, the flow is almost blocked. At the runaway case (Fig. 7d), the flow separations occur in the blade passage. The vortex magnitudes increase dramatically from turbine case (Fig. 8b) to turbine brake case (Fig. 8e).

The third dominant frequency ($4f_n$ in Fig. 6b at case G2 and Fig. 6d at case G4) in pump turbine may be caused by the blockage of flow in the blade passage. For example, there are some flow blocks at the inlet of four blade passages of runner at turbine case (Fig. 7b) and most of the blade passages are blocked at the runaway case (Fig. 7d).

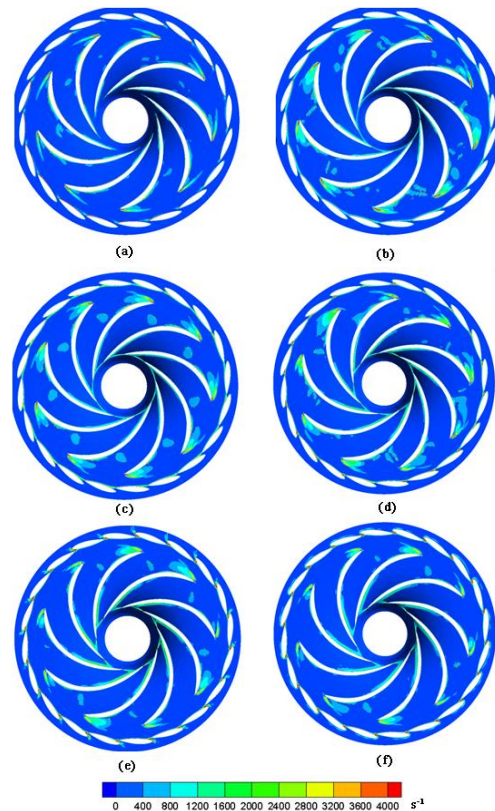


Fig. 8. Vortices distribution on the S1 stream surface of runner at different operating conditions G1-G6 (corresponding to (a)-(f) respectively).

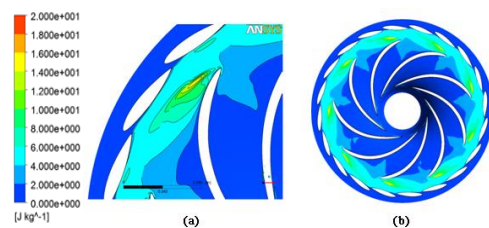


Fig. 9. Turbulent kinetic energy distributions on S1 stream surface at operating condition G1.

From Fig. 6, 8 and 9 at the inlet of runner, the velocity, the vortex and the turbulent kinetic energy are very large near the pressure surface and leading edge of the blades, leading to high pressure fluctuations on the vaneless spaces of the pump turbine. Results reveal that the pressure fluctuation only contains rather high-frequency components (e.g. the runner blade passing frequency and guide vane passing frequency). When the pump turbine runs at turbine braking mode, large vortex can be seen in the passage of the runner. The stall phenomena will increase the pressure fluctuation in the vaneless space.

5. CONCLUSIONS

In order to study the pressure fluctuation of the model pump turbine at the turbine mode, three dimensional unsteady turbulent flow simulations have been carried out using the PANS approach based on modifications of RNG $k-\varepsilon$ turbulence model under 6° opening of the guide vanes. The predicted performance and relative amplitude of peak-to-peak pressure fluctuations at time domain in the vaneless space of the pump turbine are both very close to the experimental data.

- (1) The maximum amplitude of pressure fluctuation in the vaneless space appears when the pump-turbine runs at runaway point. The amplitude of pressure fluctuation increases first then decrease as the flow rate decrease from turbine mode.
- (2) The dominate frequency of pressure fluctuation in the vaneless space is the runner blade passing frequency and the second dominate frequency is double of the runner blade passing frequency. The second dominate frequency is nearly equal to guide vane passing frequency.
- (3) The relative velocity of near the blade suction surface of the runner is considerably higher than one in other areas in runner. At the runaway case, the flow separations occur in the blade passage. The vortex magnitudes increase dramatically from turbine case to turbine brake case.
- (4) At the inlet of runner, the velocity, the vortex and the turbulent kinetic energy are very large near the pressure surface and leading edge of the blades, causing strong pressure fluctuations within the vaneless space of the pump turbine, which should be avoided during the design of pump turbines especially those operated at high head conditions.

ACKNOWLEDGMENTS

The authors would like to thank projects 51406010 supported by National Natural Science Foundation of China and project supported by open Research Fund Program of State key Laboratory of Hydroscience and Engineering, NO. sklhse-2014-E-02.

REFERENCES

- Ehrhard, J. (1999). Research on linear and nonlinear eddy viscosity turbulence models for building. Ph.D. thesis, VDI, Düsseldorf, Germany.
- Germano, M. (1992). Turbulence: The Filtering Approach. *J. Fluid Mech.* 238, 325–336.
- Girimaji, S., R. Srinivasan and E. Jeong (2003). PANS turbulence models for seamless transition between RANS and LES: fixed point analysis and preliminary results. *ASME paper FEDSM*.
- Girimaji, S. (2006). Partially-averaged navier–stokes model for turbulence: a Reynolds-averaged Navier–Stokes to direct numerical simulation bridging method. *ASME J. of Applied Mechanics* 73(2), 413–421.
- Hasmatuchi, V. M. Farhat, P. Maruzewski and F. Avellan (2009). Experimental investigation of a pump-turbine at off-design operating conditions. In *Proceedings of the 3rd International Meeting of the Workgroup on Cavitation and Dynamic Problems in Hydraulic Machinery and Systems*, Brno, Czech Republic 339-347
- Hasmatuchi, V., S. Roth, F. Botero, M. Farhat and F. Avellan (2011). Hydrodynamics of a pump-turbine at off-design operating conditions: numerical simulation. In *Proceedings of ASME-JSME-KSME Joint Fluids Engineering Conference 2011*, Hamamatsu, Japan
- Huang, H, R. F. Xiao, W. S. Liu and F. J. Wang (2013). Analysis of S characteristics and pressure pulsations in a pump-turbine with misaligned guide vanes. *ASME J. of Fluids Engineering* 135/051101-1
- Ji, B., X. W. Luo., Y. L. Wu, X. X. Peng and Y. L. Duan (2013). Numerical analysis of unsteady cavitating turbulent flow and shedding shoe vortex structure around a twisted hydrofoil. *International Journal of Multiphase Flow* 51, 33-43.
- Jung, A., J. P. Yan and M. Giese (2012). Development of a reliable very high-head pump turbine considering challenging hydrodynamics. *IOP Conf. Series: Earth and Environmental Science* 15.
- Lakshmipathy, S. (2004). *PANS Method for Turbulence simulation of high and low Reynolds number flow past a circular cylinder*. M. Sc. Thesis, Dept. of Aerospace Eng. Texas A. & M. University, USA.
- Liu, J. T., S. H. Liu, Y. K. Sun, Y. L. Wu and L. Q. Wang (2012). Three dimensional flow simulation of load rejection of a prototype pump-turbine. *Engineering with computers*
- Liu, J. T., S. H. Liu, Y. K. Sun, Y. L. Wu and L. Q. Wang (2013). Three-dimensional flow simulation of transient power interruption process of a prototype pump-turbine at pump

- mode. *J. of Mechanical Science and Technology* 27(5), 1-8.
- Mirzaei, M. and S. Krajnović, B. Basara (2015). Partially-Averaged Navier–Stokes simulations of flows around two different Ahmed bodies. *Computers and Fluids* 117, 273-286.
- Nicolet, C., N. Ruchonnet and F. Avellan (2006, Feb.). One-dimensional modeling of rotor-stator interaction in Francis pump-turbine. In *Procs of ISROMAC-11ASME*, Honolulu, USA.
- Qian, Z. D., B. Zheng, W. X. Huai and Y. H. Lee (2010). Analysis of pressure oscillations in a Francis hydraulic turbine with misaligned guide vanes. In *Procs of IME Part A J. of Power and Energy* 224(1), 139-152
- Shi, W. (2015). Numerical simulation of cavitation shedding flow around a hydrofoil using Partially-Averaged Navier-Stokes model. *International Journal of Numerical Methods for Heat and Fluid Flow* 25(4), 825-830.
- Srinivasan, R. and S. S. Girimaji (2014). Partially-Averaged Navier–Stokes Simulations of High-Speed Mixing Environment. *Journal of Fluids Engineering-Transactions of the ASME* 136(6).
- Staubli, T., F. Senn and M. Sallaberger (2008). Instability of pump-turbines during start-up in the turbine mode, Proceedings of Hydro 2008, October 6 – 8, Ljubljana, Slovenia, Paper No. 9.6.
- Wang, L. Q., J. L. Yin, Jiao and *et al.* (2011). Numerical investigation on the S characteristics of a reduced pump turbine model. *Science China Technological Sciences* 54, 1259-1266
- Wu, Y. L., S. C. Li, S. H. Liu, H. S. Dou and Z. D. Qian (2013). Vibration induced by hydraulic excitation. In *Vibration of hydraulic machinery* Springer Germany 147-233.
- Wu, Y. L., S. H. Liu, L. Zhang and H. S. Dou (2011). Simulations of unsteady cavitating turbulent flow in a Francis turbine using the RANS method and the improved mixture model of two-phase flows. *Eng. Comput* 27, 235–250
- Yakhot, V., S. A. Orszag, S. Thangam, T. B. Gatski and C. G. Speziale (1992). Development of turbulence models for shear flows by a double expansion technique. *Physics of Fluids A: Fluid Dynamics* 4, 1510.
- Yamaguchi, Y. and K. Shimmei (1984). Dynamic characteristics of reversible pump-turbine in pump storage plants. *USDE and EPRI Symposium*, Boston 89-93.
- Yan, J. P., U. Seidel and J. Koutnik (2012). Numerical simulation of hydrodynamics in a pump-turbine at off-design operating conditions in turbine mode. *IOP Conf. Series: Earth and Environmental Science* 15.
- Yan, J., J. Koutnik, U. Seidel and B. Hübner (2010). Compressible simulation of rotor-stator interaction in pump-turbines. *IOP Conf. Series: Earth and Environmental Science* 12.
- Yin, J. L., D. Z. Wang, L. Q. Wang, Y. L. Wu and X. Z. Wei (2012). Effects of water compressibility on the pressure fluctuation prediction in pump turbine. *IOP Conf. Ser.: Earth Environ. Sci.* 15.
- Yin, J. L., J. T. Liu, L. Q. Wang and X. Z. Wei (2011). Prediction of pressure fluctuations of pump turbine under off-design condition in pump mod *J. Engr. Thermophysics* 32(7), 1141-1144 (in Chinese)
- Zobeiri, A., J. L. Kueny, M. Farhat and F. Avellan (2006). Pump-turbine rotor–stator interactions in generating mode: pressure fluctuation in distributor channel. In *Proceedings of the 23rd IAHR Symposium*, Yokohama F 235.